Accuracy of Confocal and Dermoscopic Criteria for Predicting Basal Cell Carcinoma Subtype

Yunmin Zou, MD,† Rushan Xia, MD, PhD,† Shuyan Li, MD,‡ Lu Li, MM,§ Danning Zhu, MM,† Yinni Ma, MM,† Peng Wang, MD,¶ and Fei Wang, MD, PhD**

Background: The correct diagnosis of basal cell carcinoma (BCC) histopathological subtype is crucial for treatment design. Although the diagnostic accuracy of reflectance confocal microscopy (RCM) and dermoscopy for BCC has been studied, the literature of RCM and dermoscopy in predicting BCC subtype remain limited.

Objectives: To assess the diagnostic accuracy of confocal and dermoscopic criteria for predicting BCC subtype.

Methods: Confocal and dermoscopic images of histopathologically confirmed BCC were retrospectively analyzed. Multivariate and adjusted odds ratios were computed, along with sensitivity and specificity. Receiver operating characteristic (ROC) curve was plotted, and the area under the curve (AUC) was calculated.

Results: The study included 103 patients with 124 lesions. And 84 (105 lesions) were assigned to the confocal analysis group and 49 (62 lesions) to the dermoscopic analysis group. Multivariate analysis yielded three confocal models for predicting a diagnosis of nodular BCC (nBCC) with sensitivity of 91.7% and specificity of 80.7% (AUC, 0.913), superficial BCC (sBCC) with sensitivity of 82.3% and specificity of 91.5% (AUC, 0.932), and aggressive BCC (aBCC) with sensitivity of 87.5% and specificity of 97.8% (AUC, 0.945). We developed three dermoscopic models for diagnosing nBCC with sensitivity of 76.5% and specificity of 82.1% (AUC, 0.891), sBCC with sensitivity of 95.0% and specificity of 95.2% (AUC, 0.973), and aBCC with sensitivity of 62.5% and specificity of 90.7% (AUC, 0.849).

Conclusion: Both RCM and dermoscopy are reliable tools for the identification of BCC subtypes. RCM is more accurate for nBCC and aBCC, whereas dermoscopy is more accurate for sBCC.

From the *Department of Dermatology, Zhongda Hospital, School of Medicine, Southeast University, Nanjing, China; †Department of Dermatology, Wuxi No. 2 People's Hospital, Wuxi, China; ‡The Affiliated Taian City Centeral Hospital of Qingdao University, Taian, China; §Wuxi School of Medicine, Jiangnan University, Wuxi, China; and ¶Pediatric Dermatology, Dermatology Hospital of Southern Medical University, Guangzhou, China.

Supported by funding from Taian Science and Technology Innovation Development Project in 2022 (Project No. 2022NS152).

The authors declare no conflicts of interest.

Supplemental digital content is available for this article. Direct URL citations appear in the printed text and are provided in the HTML and PDF versions of this article on the journal's Web site (www.amjdermatopathology.com).

The research protocol was approved by the ethics committee of Wuxi No. 2 People's Hospital (project number Y-155).

Correspondence: Fei Wang, MD, PhD, Department of Dermatology, Zhongda Hospital, Southeast University, Nanjing, Jiangsu 210009, China (e-mail: ffwangfei@163.com).

Key Words: basal cell carcinoma, subtype, confocal microscopy, dermoscopy

(*Am J Dermatopathol* 2026;48:432–438)

INTRODUCTION

Basal cell carcinoma (BCC), the most common type of skin cancer, grows slowly and rarely metastasizes; however, the high-risk type of BCC can severely affect tissues and organs and is sometimes life threatening.[1] Current national and European guidelines recommend different treatment options of BCC according to the location, size, and histopathologic subtype of tumor.

The correct classification of histopathologic BCC subtypes is important for selecting effective treatment strategies. Histopathologic examination is the most accurate method for the diagnosis of BCC and the determination of tumor subtype. However, trauma and scars caused by operation affect the compliance of patients and delay the early diagnosis and prompt treatment of BCC. The use of noninvasive techniques for the pretherapy assessment of BCC histologic subtypes may save time, patient discomfort, and money.[2]

Dermoscopy allows visualization of the skin structure that is invisible to the naked eye, and it improves the diagnostic sensitivity and specificity for BCC.[3] Several studies have described the different structures characteristic of BCC and BCC subtypes observed under dermoscopy with different results.[4–6] Reflectance confocal microscopy (RCM) is an innovative technology that enables swift skin imaging with a level of detail approaching histologic resolution.[7] RCM serves as an effective method for the diagnosis of BCC.[8–10] Several RCM criteria have been reported for predicting BCC subtypes.[11,12] However, there are few reports on the accuracy of dermoscopy and RCM for predicting BCC subtype.

The aim of this study was to evaluate and compare the diagnostic accuracy of predefined confocal criteria and dermoscopic criteria for predicting BCC histopathologic subtype. We also developed multivariate predictive models for predicting BCC subtype for RCM and dermoscopy.

PATIENTS AND METHODS

Study Patients

A retrospective study was conducted at a tertiary hospital dermatology unit between January 2018 and December 2023 after obtaining institutional ethical clearance. Inclusion and exclusion criteria: Patients >18 years of age with available records of clinical findings and high-quality dermoscopy or RCM imaging data at the workstation were

included. All patients underwent surgical resection and had clear BCC histopathologic subtypes. Patients were excluded if they had incomplete clinical data, poor-quality images, or if the pathologic classification was not defined.

Evaluation of Confocal and Dermoscopic Images

RCM images were acquired using a confocal microscope (Vivascope 1500, Lucid Technologies, Rochester, NY) at a laser wavelength of 830 nm with an adjustable power range of 0–22 mW. RCM characteristics were evaluated by 2 experienced physicians. The RCM criteria used in this study were as follows: keratinocyte atypia, streaming of the epidermis, cords connected to the epidermis, ulceration, large tumor islands (diameter >300 μm), small tumor islands (diameter <300 μm), peripheral palisading, clefting, dark silhouette, onion-like structures, collagen surrounding tumor islands, increased vascularization, inflammation, intratumoral dendritic cells, and melanin granules.[9–12]

Dermoscopic images were captured using German FotoFinder equipment (FotoFinder bodystudio ATBM). Dermoscopic parameters evaluated by 2 experienced physicians were selected based on previous findings and are as follows: vascular structures including arborizing vessels and superficial (short) fine telangiectasia; pigmented structures including blue–gray ovoid nests, multiple blue–gray globules, maple leaf-like areas, spoke-wheel areas, and concentric structures; nonvascular and nonpigmented structures including ulceration, multiple small erosions, shiny white–red structureless areas, and white streaks.[3,5,6]

Histologic Analysis

The classification of BCC histopathologic subtypes was performed by 2 experienced pathologists who were masked to confocal and dermoscopic results. All lesions were histologically classified as superficial basal cell carcinoma (sBCC), nodular basal cell carcinoma (nBCC), and aggressive BCCs (aBCCs), which include micronodular BCC (mnBCC), infiltrative BCC (iBCC), and basosquamous carcinoma (BSC). The diagnosis of mixed-type histopathologic (2 or more growth patterns) subtype was made according to the histologic classification of tissues with >50% components.

Statistical Analysis

Statistical analysis was performed using SPSS software (version 23.0). Categorical variables were compared using Fisher Exact Test (frequency [N, %]). The accuracy of predefined confocal criteria and dermoscopic criteria for the diagnosis of BCC subtypes was assessed using a logistic regression model. Data are presented as odds ratio (OR) and 95% confidence interval (95% CI). $P < 0.05$ was determined to be statistically significant. Sensitivity and specificity were extracted from classification tables. A receiver operating characteristic (ROC) curve was generated for the model, and a comprehensive analysis of prognostic factors specific to each BCC histologic subtype was performed. The area under the curve (AUC) was calculated to evaluate the model's accuracy. The alpha level was designated as 0.05.

RESULTS

Patient Characteristics

A total of 140 cases of potentially eligible BCCs were identified through a comprehensive search of an electronic image database and a meticulous review of medical records within the institution. According to the inclusion and exclusion criteria, 4 cases were excluded because of poor-quality images, 22 cases because of lack of histopathologic results, and 11 cases because of a non-BCC histopathologic diagnosis.

Finally, 103 patients (mean age, 64.8 ± 12.1 years; range: 30–89 years) with 124 lesions, including 37 sBCCs, 68 nBCCs, and 19 aBCCs (11 mnBCCs, 7 iBCCs, and 1 BSC), were analyzed. Of these, 84 patients (105 lesions) including 34 sBCCs, 55 nBCCs, and 16 aBCCs (10 mnBCCs, 5 iBCCs, and 1 BSC) were subjected to confocal analysis. Dermatoscopic analysis was performed on 49 patients (62 lesions), including 21 sBCCs, 31 nBCCs, and 10 aBCCs (6 mnBCC, 3 iBCCs, and 1 BSC). In total, 30 patients with 43 lesions were both analyzed by RCM and dermoscopy, including 18 sBCCs, 18 nBCCs, and 7 aBCCs (5 mnBCCs and 2 iBCCs). The mean size of the lesions was 9.5 ± 0.58 mm (range, 2–45 mm). There were 86 lesions on the head and face (69.4%), 23 lesions on the trunk (18.5%), 12 lesions on the limbs (9.7%), and 3 lesions on the vulva (2.4%).

Evaluation of Confocal and Dermoscopic Features According to BCC Subtype

The results of the evaluation of confocal and dermoscopic features are given in **Supplemental Digital Content 1** (see **Tables S1 and S2**, http://links.lww.com/AJDP/A181), respectively. Confocal evaluation of sBCCs (Fig. 1) showed keratinocyte atypia (29/34 [85.29%]), cords connected to the epidermis (26/34 [76.47%]), streaming of the epidermis (17/34 [50%]), and peripheral palisading (18/34 [52.94%]). Large tumor islands (27/55 [49.09%]), peripheral palisading (41/55 [74.55%]), and clefting (36/55 [65.45%]) were the characteristic features of nBCC by confocal evaluation (Fig. 2). The representative features of aBCCs (Fig. 3) were small tumor islands (11/16 [68.75%]), a dark silhouette (6/16 [37.50%]), and collagen surrounding tumor islands (4/16 [25%]). All BCC subtypes showed high rates of increased vascularization, inflammation, and intratumoral dendritic cells. The proportion of melanin granules in sBCCs was significantly lower than that in nBCCs and aBCCs. Comparison of the RCM characteristics of the 3 subtypes and statistical analysis showed significant variation in the 12 features among subtypes ($P < 0.05$) except inflammation, ulceration, and increased vascularization.

In the dermoscopic analysis, the prevalent diagnostic features of sBCC (Fig. 1) were maple leaf-like areas (12/21 [57.14%]), superficial (short) fine telangiectasias (10/21 [47.62%]), shiny white–red structureless areas (18/21 [85.71%]), and multiple small erosions (14/21 [66.67%]). In nBCC (Fig. 2), the representative features were arborizing vessels (28/31 [90.32%]), blue–gray ovoid nests (23/31 [74.19%]), and ulceration (22/31 [70.97%]). Finally, the most common criteria for aBCC (Fig. 3) were arborizing vessels (8/

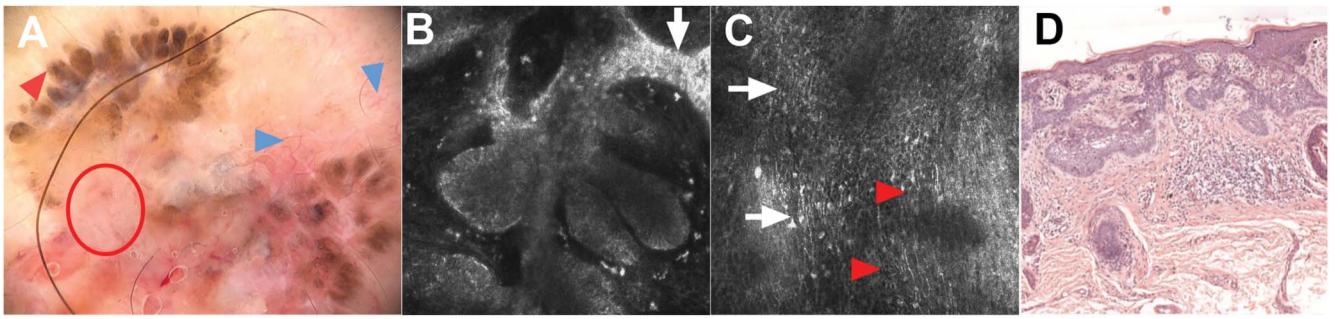

FIGURE 1. Superficial basal cell carcinoma (sBCC). A, Dermatoscopy demonstrated the presence of maple leaf-like structures (red arrow), superficial (short) fine telangiectasia (blue arrows), and shiny white–red structureless areas (red circle). B, Reflectance confocal microscopy (RCM) determined the existence of cords connected to the epidermis (white arrow). C, RCM revealed the streaming epidermis (white arrows) and atypical features in keratinocytes (red arrows). D, Histopathology of sBCC (HE, ×100).

10 [80%]), multiple blue–gray globules (6/10 [60%]), and white streaks (5/10 [50%]). In all BCC subtypes, blue–gray ovoid nests and shiny white–red structureless areas were observed at high frequency. Comparison of the dermoscopic features between the 3 groups showed significant variation ($P < 0.05$) in arborizing vessels, maple leaf-like areas, ulceration, and multiple small erosions.

Multinomial Logistic Regression Analysis of Confocal and Dermoscopic Criteria for the Classification of BCC Subtype

Twelve RCM parameters were incorporated into the multivariate analysis within an adjusted model (Supplemental Digital Content 1 (see Table S3, http://links.lww.com/AJDP/

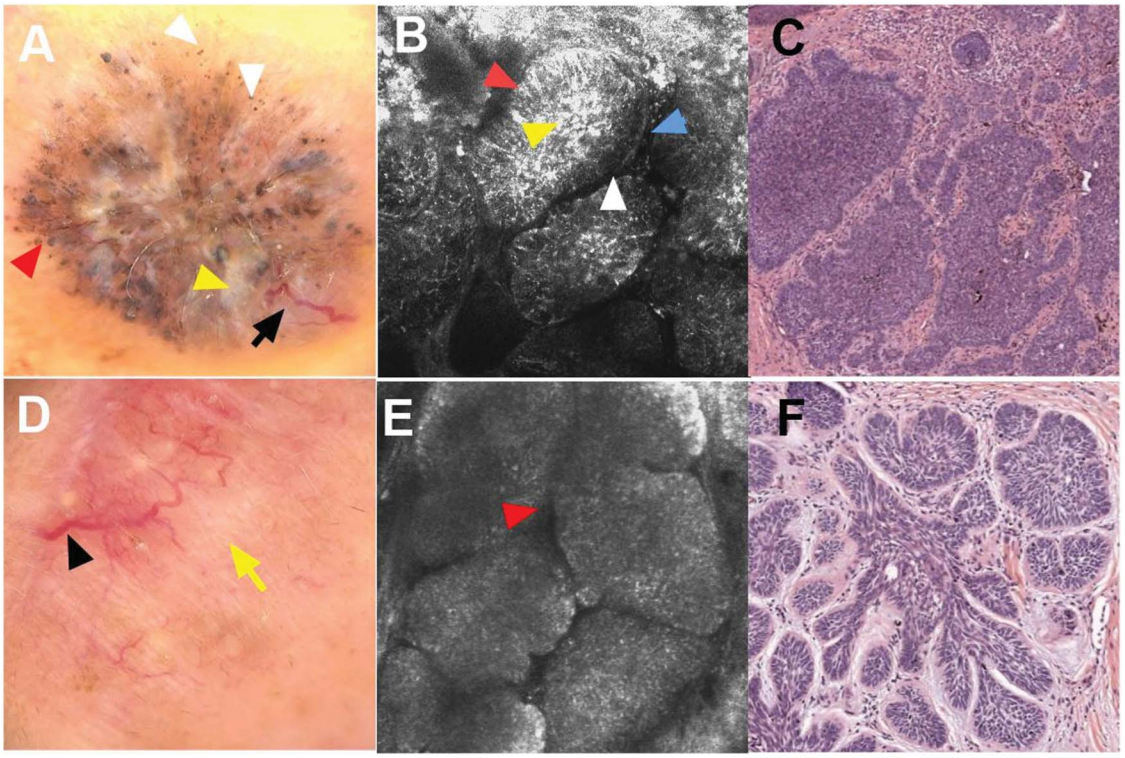

FIGURE 2. Nodular basal cell carcinoma (nBCC). A, Dermatoscopy of a pigmented nBCC showing blue–gray ovoid structures (red arrow), arborizing vessels (black arrow), multiple blue–gray globules (white arrows) and white structureless areas (yellow arrow). B, Reflectance confocal microscopy (RCM) revealed large tumor islands, peripheral palisading (red arrow), clefting (white arrow), melanin granules (yellow arrow), and increased vascularization (blue arrow). C, Histopathology revealed large basaloid islands with melanophages (HE, ×100). (D) Dermatoscopy of hypopigmented nBCC showed large arborizing vessels (black arrow) and white–red structureless areas (yellow arrow). E, RCM revealed large tumor islands with no melanophages (red arrow). F, Histopathology revealed large basaloid islands without melanophages (HE, ×100).

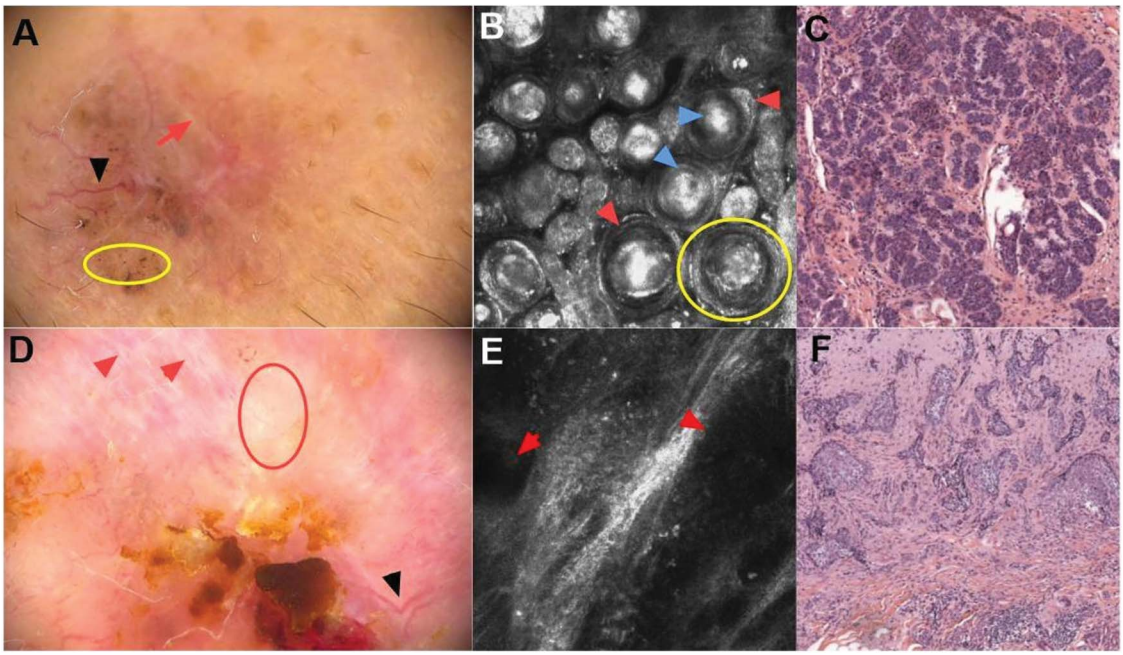

FIGURE 3. Aggressive basal cell carcinoma (aBCC). A, Dermatoscopy of mnBCC showed arborizing vessels (black arrow), multiple blue–gray globules (yellow circle), and white streaks (white arrow). B, Reflectance confocal microscopy (RCM) of mnBCC revealed small tumor islands (blue arrow), onion-like structures (yellow circle), and collagen surrounding tumor islands (red arrow). C, Histopathology of an mnBCC with multiple small tumor islands (HE, ×100). D, Dermatoscopy of iBCC revealed arborizing vessels (black arrow), white structureless areas (red circle) and white streaks (red arrow). E, RCM of iBCC revealed multiple dark silhouettes (red arrow). F, Histopathology of iBCC with infiltrative tumor islands (HE, ×100).

A181), which correctly classified 82.9% of original grouped cases. When aBCC was used as the reference group, nBCC had a 34-fold higher likelihood of showing peripheral palisading (95% CI: 2.013–602.040), and a 4-fold higher likelihood of showing clefting (95% CI: 0.356–47.484). When nBCC was used as the reference group, sBCC had a 41-fold higher likelihood of having cords connected to the epidermis (95% CI: 5.734–306.931). aBCC was 19-fold more likely to show onion-like structures (95% CI: 0.984–395.74) and 8-fold more likely to show a dark silhouette (95% CI: 0.427–180.108).

Multivariate analysis was performed by incorporating 10 dermoscopic parameters into an adjusted model in Table S3, which correctly classified 87.1% of the originally grouped cases. When aBCC was used as the reference group, nBCC was 10-fold more likely to show blue–gray ovoid nests (95% CI: 0.765–136.996). sBCC was 142-fold more likely to show maple leaf-like areas (95% CI: 1.856–10970.825) and 33-fold more likely to show blue–gray ovoid nests (95% CI: 0.931–1210.368). When nBCC was used as the reference group, sBCC had a 71-fold higher likelihood of showing maple leaf-like areas (95% CI: 1.297–3890.414) and a 19-fold higher likelihood of showing shiny white–red structureless areas (95% CI: 0.125–3069.669). When sBCC was used as the reference group, aBCC was 78-fold more likely to show arborizing vessels (95% CI: 1.948–3161.281).

Accuracy of Dermoscopic and Confocal Criteria for Predicting BCC Subtype

Three separate binary logistic regression models were developed for BCC subtypes using 12 confocal criteria as independent variables. Multivariate analysis was used to determine the effect of confocal criteria on the various subtypes of BCC (Table 1). The ROC for the 3 models is shown in Figures 4A–C. The model showed high diagnostic accuracy for nBCC, with sensitivity of 91.7% and specificity of 80.7% (AUC: 0.913). The most significant predictor of the probability of nBCC was the appearance of peripheral palisading (OR: 12.598; AUC = 0.663), followed by clefting (OR: 2.581; AUC = 0.687). The model showed diagnostic accuracy, with sensitivity of 82.3% and specificity of 91.5% for sBCC (AUC: 0.932). The strongest factor was the presence of cords connected to the epidermis (OR: 25.939; AUC = 0.833), followed by streaming of the epidermis (OR: 2.469; AUC = 0.673). The model showed diagnostic accuracy, with sensitivity of 87.5% and specificity of 97.8% for aBCC (AUC: 0.945). The strongest factor was the presence of onion-like structures (OR: 24.973; AUC = 0.623), followed by collagen surrounding tumor islands (OR, 15.988; AUC = 0.654), dark silhouettes (OR: 15.360; AUC = 0.643), and small tumor islands (OR: 4.316; AUC = 0.647).

Three separate binary logistic regression models with 10 dermoscopy criteria as independent variables were

TABLE 1. Multivariate Logistic Regression Analysis of Confocal Criteria Predictors

	Variables	*P*	OR (95% CI)
Nodular	Cords connected to the epidermis	<0.001*	0.011 (0.002–0.083)
	Big tumor islands	0.532	1.616 (0.359–7.275)
	Peripheral palisading	0.01*	12.598 (1.836–86.448)
	Clefting	0.202	2.581 (0.601–11.093)
Superficial	Streaming of the epidermis	0.286	2.469 (0.469–12.997)
	Cords connected to the epidermis	<0.001*	25.939 (4.666–144.209)
Aggressive	Small tumor islands	0.208	4.316 (0.444–41.951)
	Dark silhouette	0.098	15.360 (0.603–391.049)
	Peripheral palisading	0.028*	0.030 (0.001–0.690)
	Onion-like structures	0.041*	24.973 (1.144–545.229)
	Collagen surrounding tumor islands	0.075	15.988 (0.753–339.283)

Independent variables entered in each multivariate logistic regression model were as follows: keratinocyte atypia, streaming of the epidermis, cords connected to the epidermis, small tumor islands, big tumor islands, dark silhouette, peripheral palisading, clefting, onion-like structures, collagen surrounding tumor islands, intratumoral dendritic cells, and melanin granule.

*Indicates logistic regression analysis significant differences ($P < 0.05$).

developed for BCC subtypes. We used multivariate analysis to determine the effect of dermoscopic parameters on BCC subtypes (Table 2). The ROC for the 3 models is shown in Figures 4D–F. The model showed diagnostic accuracy, with sensitivity of 76.5% and specificity of 82.1% for nBCC (AUC: 0.891). The strongest predictors for the diagnosis of nBCC were ulceration (OR: 11.843; 95% CI: 1.712–81.953; $P = 0.012$, AUC = 0.774), followed by arborizing vessels (OR: 6.238; 95% CI: 0.980–39.705; $P = 0.053$, AUC = 0.758). The model showed diagnostic accuracy, with sensitivity of 95.0% and specificity of 95.2% for sBCC (AUC: 0.973). The strongest factor was the presence of maple leaf-like areas (OR: 37.352; AUC = 0.676), followed by multiple small erosions (OR: 10.574; AUC = 0.785). The model showed sensitivity of 62.5% and specificity of 90.7% for the diagnosis of aBCC (AUC: 0.849). The strongest factor was the presence of arborizing vessels (OR: 7.010; AUC = 0.592), followed by white streaks (OR: 4.745; AUC = 0.606).

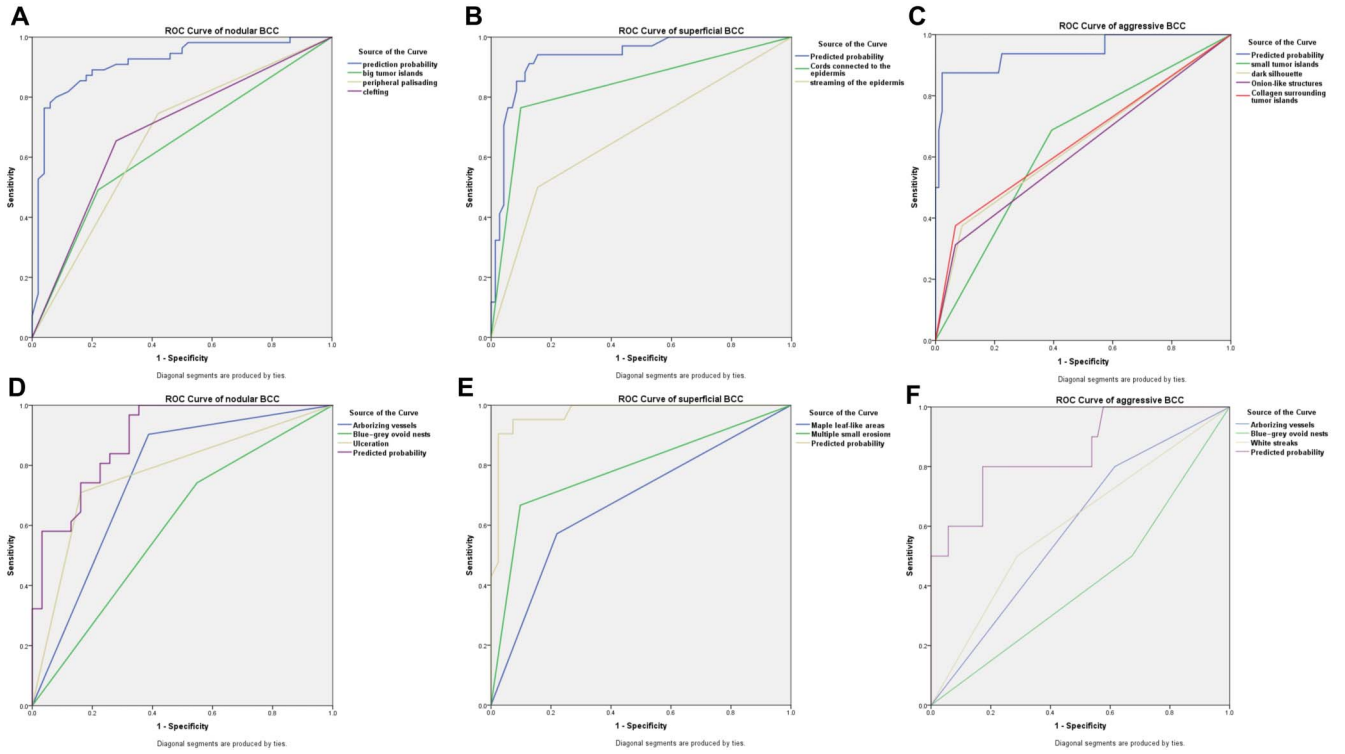

FIGURE 4. Receiver operating characteristic (ROC) curve. A–C, Three separate models were created for nBCC, sBCC, and aBCC, depending on dichotomous RCM variables. D–F, Three separate models were created for nBCC, sBCC, and aBCC, depending on dichotomous dermoscopy variables.

TABLE 2. Multivariate Logistic Regression Analysis of Dermoscopic Criteria Predictors

	Variables	*P*	OR (95% CI)
Nodular	Arborizing vessels	0.053	6.238 (0.980–39.705)
	Blue–gray ovoid nests	0.284	2.501 (0.466–13.420)
	Concentric structures	0.55	2.544 (0.119–54.281)
	Ulceration	0.012*	11.843 (1.712–81.953)
Superficial	Arborizing vessels	0.021*	0.027 (0.001–0.583)
	Superficial (short) fine telangiectasias	0.429	2.987 (0.199–44.589)
	Maple leaf-like areas	0.019*	37.352 (1.795–777.430)
	Multiple small erosions	0.208	10.574 (0.269–415.625)
Aggressive	Arborizing vessels	0.111	7.010 (0.637–77.119)
	Blue–gray ovoid nests	0.043*	0.091 (0.009–0.929)
	White streaks	0.165	4.745 (0.526–42.802)
	Multiple blue–gray globules	0.330	2.753 (0.359–21.354)

Independent variables entered in each multivariate logistic regression model were as follows: arborizing vessels, superficial (short) fine telangiectasias, blue–gray ovoid nests, multiple blue–gray globules, maple leaf-like areas, concentric structures, ulceration, multiple small erosions, shiny white–red structureless areas, and white streaks.
*Indicates logistic regression analysis significant differences ($P < 0.05$).

DISCUSSION

In this investigation, we evaluated and compared the predictive accuracy of confocal microscopy and dermoscopy for identifying different BCC subtypes. The results indicate that RCM and dermoscopy are both valid tools for diagnosing BCC subtype with high sensitivity and specificity. RCM is superior to dermoscopy for predicting the diagnosis of nBCC with sensitivity of 91.7% and specificity of 80.7%, and aBCC with sensitivity of 87.5% and specificity of 97.8%. Dermoscopy is superior to RCM for predicting the diagnosis of sBCC, with sensitivity of 95.0% and specificity of 95.2%.

Confocal microscopy differences between BCC subtypes were reported previously.[11–13] The hallmarks of sBCC are the presence of cords connected to the epidermis[11,12] and epidermal streaming.[11,14,15] Solar elastosis and the presence of tumor nests proximal to or adjacent to the basal cell layer are distinctive characteristics of sBCC.[13] The findings of this study are consistent with the literature.[11,12] The presence of cords connected to the epidermis was 24-fold more likely in sBCC than in non-sBCC ($P < 0.001$*, Table 1) and 40-fold more likely in sBCC than in nBCC ($P < 0.001$*, Table S3). The AUC of cords connected to the epidermis for predicting the diagnosis of sBCC was 0.833 (Fig. 4B). The presence of big tumor islands and clefting are predictors of nBCC.[11] However, in this study, the strongest predictor of nBCC diagnosis was the presence of peripheral palisading (OR: 12.598; AUC: 0.663), followed by clefting (OR: 2.581; AUC: 0.687).

A previous study reported that the primary features of RCM in nBCC and mnBCC were tumor nests with peripheral palisading, branch-like structures, fibrotic septa, and increased vascular diameter.[13] The dimensions, configuration, and site of the tumor nests can further distinguish nBCC from mnBCC.[13] In this study, mnBCC was classified as aBCC, and large tumor islands were present in only 1 case (1/10). The presence of small tumor islands and the absence of large tumor islands may be a strong factor for mnBCC. A confocal pattern of dark silhouettes is a characteristic of iBCC.[11,12] The present findings were inconsistent with those of a previous report,[12] because we found that collagen surrounding tumor islands (OR: 15.988; AUC = 0.654) was a strong predictor of aBCC diagnosis, followed by onion-like structures (OR: 24.973; AUC = 0.623) and dark silhouettes (OR: 15.360; AUC = 0.643), which may be on account of mnBCC accounting for 10 of 16 of aBCCs. This model correctly classified 82.9% of originally grouped cases in the 3 subtypes analysis, which was superior to the previous model showing accuracy of 74.4%.[11] Many studies have reported the diagnostic accuracy of RCM for diagnosing BCC, with sensitivity estimates varying between 83% and 100% and specificity oscillating within the range of 78%–97%.[8,13–17] However, there are few reports on the accuracy including specificity and sensitivity for diagnosing BCC subtype. Few studies reported the classification probability of originally grouped cases without specificity and sensitivity.[11,12] According to the outcomes of the multivariate analysis, we built 3 models for RCM that showed high accuracy for predicting nBCC (AUC = 0.913), sBCC (AUC = 0.932), and aBCC (AUC = 0.945). In addition, this study provided the AUC of the strong predicting factor, which has not been reported in the literature.

Previous studies reported the dermoscopic features that are investigated in BCC and its subtypes with different results.[6,11,18–20] The most common dermoscopic feature for the diagnosis of BCC is blood vessels, particularly arborizing vessels or short fine telangiectasia, which is observed in 51%−75% of tumors and is specific to BCC subtypes.[6] The blood vessels appeared in 80.6% of the tumors in our study. Consistent with previous reports, arborizing vessels was the strong predicting factor for nBCC (OR: 6.238), and short fine telangiectasia was the strong predicting factor for sBCC (OR: 2.987).[11,20,21] A previous study reported that pigmented structures are present in 36% of cases of BCCs and its histopathologic subtypes,[6] whereas they were identified in 88.7% of all grouped cases in this study. In the multivariate analysis, maple leaf-like areas were the strong predicting factor for sBCC (OR: 37.352; AUC = 0.676), which is in agreement with previous studies.[6,19,20] Blue–gray ovoid nests were a positive predictive factor for the diagnosis of nBCC (OR: 10.239) in line with

a previous report,[6] and a negative predicting factor for aBCC (OR: 0.091). Multiple blue–gray globules were identified in 60% of aBCCs (100% of mnBCCs), which was a positive predictive factor for aBCC (OR: 2.753), which is consistent with the literature.[22] Multiple blue–gray globules were histopathologically related to small tumor nests in the dermis[23] and confocally associated with small tumor islands, which may indicate a diagnosis of mnBCC.[22] For nonvascular and nonpigmented structures, ulceration was a positive predictive factor for nBCC (OR: 11.843) in the multivariate analysis, as described previously.[6] Consistent with a previous study,[19] maple leaf-like areas, short fine superficial telangiectasia, multiple small erosions, and shiny white–red structureless areas were positive predictors of sBCC, whereas the presence of arborizing vessels was a negative predictor of sBCC in Table 2. We built a model for predicting the diagnosis of sBCC with higher accuracy (sensitivity of 95.0% and specificity of 95.2%) than a previously reported model (sensitivity of 81.9% and specificity of 81.8%).[19] We also developed models for the diagnosis of nBCC (AUC = 0.891) and aBCC (AUC = 0.849), and identified strong predictive factors for each BCC subtype (Fig. 4). According to previous meta-analyses, confocal microscopy has a sensitivity 0.97 and specificity 0.93 for the diagnosis of BCC, whereas dermoscopy showed a pooled sensitivity of 0.91 and specificity of 0.95.[3,8] In this study, RCM showed better diagnostic accuracy for nBCC and aBCC, whereas dermoscopy showed higher diagnostic accuracy for sBCC. To the best of our knowledge, this is the first study to evaluate and compare the diagnostic accuracy of RCM and dermoscopy for sBCC, nBCC, and aBCC.

The major limitation of this study was the small number of patients, particularly in aBCC. Furthermore, the diagnostic accuracy results were based on data from one center, which may not reflect all real-life clinical situations. Finally, this study was a retrospective design, which cannot reflect all confocal and dermoscopic features of BCC.

In conclusion, we confirmed specific confocal and dermoscopic criteria for different BCC subtypes and developed prediction models for the identification of BCC subtypes based on RCM and dermoscopy. Both RCM and dermoscopy showed high accuracy for predicting BCC subtypes, which can provide guidance for the treatment of BCC. Further studies are needed to confirm the results. A prospective, multicenter and larger sample size study is needed to improve the diagnostic accuracy of pretherapy subtype classification of BCC.

REFERENCES

1. Peris K, Fargnoli MC, Kaufmann R, et al. European consensus-based interdisciplinary guideline for diagnosis and treatment of basal cell carcinoma-update 2023. *Eur J Cancer.* 2023;192:113254.
2. Kadouch DJ, Elshot YS, Zupan-Kajcovski B, et al. One-stop-shop with confocal microscopy imaging vs. standard care for surgical treatment of basal cell carcinoma: an open-label, noninferiority, randomized controlled multicentre trial. *Br J Dermatol.* 2017;177:735–741.
3. Reiter O, Mimouni I, Gdalevich M, et al. The diagnostic accuracy of dermoscopy for basal cell carcinoma: a systematic review and meta-analysis. *J Am Acad Dermatol.* 2019;80:1380–1388.
4. Ceder H, Backman E, Marghoob A, et al. Importance of both clinical and dermoscopic findings in predicting high-risk histopathological subtype in facial basal cell carcinomas. *Dermatol Pract Concept.* 2024;14:e2024212.
5. Popadic M, Brasanac D. The use of dermoscopy in distinguishing the histopathological subtypes of basal cell carcinoma: a retrospective, morphological study. *Indian J Dermatol Venereol Leprol.* 2022;88:598–607.
6. Reiter O, Mimouni I, Dusza S, et al. Dermoscopic features of basal cell carcinoma and its subtypes: a systematic review. *J Am Acad Dermatol.* 2021;85:653–664.
7. Woliner-van der Weg W, Peppelman M, Elshot YS, et al. Biopsy outperforms reflectance confocal microscopy in diagnosing and subtyping basal cell carcinoma: results and experiences from a randomized controlled multicentre trial. *Br J Dermatol.* 2021;184:663–671.
8. Kadouch DJ, Schram ME, Leeflang MM, et al. In vivo confocal microscopy of basal cell carcinoma: a systematic review of diagnostic accuracy. *J Eur Acad Dermatol Venereol.* 2015;29:1890–1897.
9. Longo C, Guida S, Mirra M, et al. Dermatoscopy and reflectance confocal microscopy for basal cell carcinoma diagnosis and diagnosis prediction score: a prospective and multicenter study on 1005 lesions. *J Am Acad Dermatol.* 2024;90:994–1001.
10. Stevens HP, Pampena R, Farnetani F, et al. Reflectance confocal microscopy in diagnosing basal cell carcinoma in the UK: a prospective observational single-centre trial. *Br J Dermatol.* 2025;192:206–214.
11. Longo C, Lallas A, Kyrgidis A, et al. Classifying distinct basal cell carcinoma subtype by means of dermatoscopy and reflectance confocal microscopy. *J Am Acad Dermatol.* 2014;71:716–724.e1.
12. Lupu M, Popa IM, Voiculescu VM, et al. A retrospective study of the diagnostic accuracy of in vivo reflectance confocal microscopy for basal cell carcinoma diagnosis and subtyping. *J Clin Med.* 2019;8:449.
13. Peppelman M, Wolberink EAW, Blokx WAM, et al. In vivo diagnosis of basal cell carcinoma subtype by reflectance confocal microscopy. *Dermatology.* 2013;227:255–262.
14. Guitera P, Menzies SW, Longo C, et al. In vivo confocal microscopy for diagnosis of melanoma and basal cell carcinoma using a two-step method: analysis of 710 consecutive clinically equivocal cases. *J Invest Dermatol.* 2012;132:2386–2394.
15. Nori S, Rius-Diaz F, Cuevas J, et al. Sensitivity and specificity of reflectance-mode confocal microscopy for in vivo diagnosis of basal cell carcinoma: a multicenter study. *J Am Acad Dermatol.* 2004;51:923–930.
16. Castro RP, Stephens A, Fraga-Braghiroli NA, et al. Accuracy of in vivo confocal microscopy for diagnosis of basal cell carcinoma: a comparative study between handheld and wide-probe confocal imaging. *J Eur Acad Dermatol Venereol.* 2015;29:1164–1169.
17. Longo C, Farnetani F, Ciardo S, et al. Is confocal microscopy a valuable tool in diagnosing nodular lesions? A study of 140 cases. *Br J Dermatol.* 2013;169:58–67.
18. Emiroglu N, Cengiz FP, Kemeriz F. The relation between dermoscopy and histopathology of basal cell carcinoma. *An Bras Dermatol.* 2015;90:351–356.
19. Lallas A, Tzellos T, Kyrgidis A, et al. Accuracy of dermoscopic criteria for discriminating superficial from other subtypes of basal cell carcinoma. *J Am Acad Dermatol.* 2014;70:303–311.
20. Suppa M, Micantonio T, Di Stefani A, et al. Dermoscopic variability of basal cell carcinoma according to clinical type and anatomic location. *J Eur Acad Dermatol Venereol.* 2015;29:1732–1741.
21. Micantonio T, Gulia A, Altobelli E, et al. Vascular patterns in basal cell carcinoma. *J Eur Acad Dermatol Venereol.* 2011;25:358–361.
22. Camela E, Ilut Anca P, Lallas K, et al. Dermoscopic clues of histopathologically aggressive basal cell carcinoma subtypes. *Medicina (Kaunas).* 2023;59:349.
23. Alvarez-Salafranca M, Ara M, Zaballos P. Dermoscopy in basal cell carcinoma: an updated review. *Actas Dermosifiliogr (Engl Ed).* 2021;112:330–338.